(BL7A)

Soft X-ray Absorption Study of Al-based Quasicrystals and Alloys

M. MORI, T. MATSUKAWA‡, T. ONDA and M. FURUTA

School of Informatics and Sciences, Nagoya University, Nagoya 464-8601
‡ Naruto University of Education, Naruto, Tokushima

Since the discovery of an icosahedral phase (i-phase) in Al-Mn alloys by Shechtman *et al.* [1], there have been reported a large number of studies about the electronic properties of icosahedral materials in spite of remaining the arrangement of the atoms in an i-phase unclear. By intuition the pseudogap structure can be interpreted in terms of the nearly-free-electron-like energy gap inferred from the strong diffraction spots, which may be related to the stability of the i-phase. Friedel pointed out the possibility that the pseudogap structure can be enhanced by a crossing effect of 3d state with the nearly-free-electron-like state, and the stability would be augmented in an i-phase system containing transition metals by the crossing effect at about E_F which enhances the energy gap of the Brillouin zone. Recently a pseudogap-like anomaly in the DOS structure near E_F was directly confirmed with the photoemission study of an Al-Cu-Fe i-phase by Mori *et al.* [2]. A number of authors have reported about the structures of quasicrystals. But the final answers has not reported yet. More than half materials making quasicrystals has a Al element for the main component. We should have the information around a local structure around aluminum at least. But we dot know the EXAFS study of an Al element. We have already tried to study EXAFS about Al, but in the results many goast peaks appear.

The purpose is to observe soft x-ray absorption study to search the Al K edge and discuss about Al electron states and Al local structures on the stability of the i-phase. The sample – an Al-Pd-Mn i-phase quasicrystal – was an ingot prepared by the same method in ref. [3]. It was confirmed that the specimen used with this study consists of only *a usually-reported F-type i-phase* but does not contain the other phases. Photo yield studies were performed with a spectrometer on beam-line BL-7A. All measurements were carried out at room temperature. The clean surface of the specimen was obtained by scraping with a diamond file in a vacuum of $2 - 4 \times 10^{-8}$ Torr. A spectral dependence of incident radiation was determined from a photoelectric yield spectrum of gold.

At first, we try to get a yield spectra of pure aluminum ingot. But we cannnot have good data of aluminum K-edge.

[1] Shechtman D., Blech I., Gratias D. and Cahn J. W., 1984, *Phys. Rev. Lett.*, **53**, 1951

[2] Mori M., Matsuo S., Ishimasa T., Matsuura T., Kamiya K., Inokuchi H. and Matsukawa T., 1991, *J. Phys.: Condens. Matter*, **3**, 767 *ibid.*, 1992, *J. Phys.: Condens. Matter*, **4**, L157

[3] Ishimasa T. and Mori M., 1992, *Phil. Mag.*, **B18**, L175

(BL7A)

Zr L_3-Edge XANES analysis of $Fe/SO_4^{2-}/ZrO_2$ catalyst.

Tomomi Kosaka, Yoshiaki Takahashi, Ayako Matsuyoshi, Atsuyuki Miyaji and Sadao Hasegawa

Department of Chemistry, Tokyo Gakugei University, Koganei, Tokyo 184-8501

Introduction

Sulfated ZrO_2 was known as the solid superacid which has catalytic function of skeletal isomerization for alkane. Recently, an iron and a manganese ion were promoted to the sulfated ZrO_2 was found to be several times more active than unpromoted one by Hsu et al [1]. This catalyst was later studied by several researchers [2-5] and confirmed its remarkable activity. However, the effect of Fe and Mn promoters to the activity for skeletal isomerization was still unknown. In this work, we prepared sulfated Fe/ZrO_2 and investigated its electron structure using X-ray absorption near edge spectroscopy at Zr L_3-edges.

Experimental

The sample powder was obtained by the following procedure. Aqueous ammonia (25% NH_3) added slowly to a solution of $ZrOCl_2 \cdot 8H_2O$ until pH=8. After the precipitated $Zr(OH)_4$ gel was washed by a deionized water, dried at 383K for 24h. Fe/ZrO_2 was prepared in a solution of 3.74mol/l $Fe(NO_3)_2$ for 6h and dried, then calcined at 473～1073K for 2h in air. Secondary, the obtained powder was stirred in a solution of 0.5mol/l H_2SO_4 for 6h and dried at 383K for 24h in air, calcined for 2h in air at 100K below than the temperature Fe/ZrO_2 prepared, then sulfated Fe/ZrO_2 powder was obtained. In this report, the secondary calcination temperature was indicated on the case of sulfated Fe/ZrO_2.

Zr L_3-edge XANES analysis was carried out on the BL7A at UVSOR, Institute for Molecular Science, Okazaki, Japan. Spectra were recorded in a total electron yield mode at room temperature, using Ge(111) double crystal monochromator.

Results and Discussion

Fig.1 and 2 shows Zr L_3-edge spectra of sulfated ZrO_2 [6] and sulfated Fe/ZrO_2 calcined at different temperature. The two peaks (2221, 2223eV) which were correspond to transfer from $2s_{3/2}$ to t_{2g} and e_g of 4d orbital, observed in these spectra. As reported previously, sulfated ZrO_2 has a characteristic electron structure when it was most active for catalytic reaction[6]. A same phenomenon was observed in Fig.2. The spectra of sulfated Fe/ZrO_2 which calcined at 673K and 773K was similar one of sulfated ZrO_2 calcined at 873K. It was indicated that Zr atom has high oxidation state due to S atom in SO_4 ion was acted as electron acceptor when the highly activity for catalytic reaction was observed. Accordingly, we measured the conversion of sulfated Fe/ZrO_2 to skeletal isomerization for n-butane at 473K. As expected, the best conversion was observed in sulfated Fe/ZrO_2 which calcined at 673K. However, the calcination temperature for most active state was about 100～200K lower than that of sulfated ZrO_2. On the other hand, the absolute value of best conversion on sulfated Fe/ZrO_2 (about 4%) was considerably low compared to sulfated ZrO_2(about 20%). This low activity of sulfated Fe/ZrO_2 was caused by small surface area due to two

times of the calcination. From these results, it was confirmed that the calcination temperature needs for high oxidation state, that is, most active state was decreased by Fe addition in this catalysis series. However, its generation mechanism of superacidic sites were still unknown.

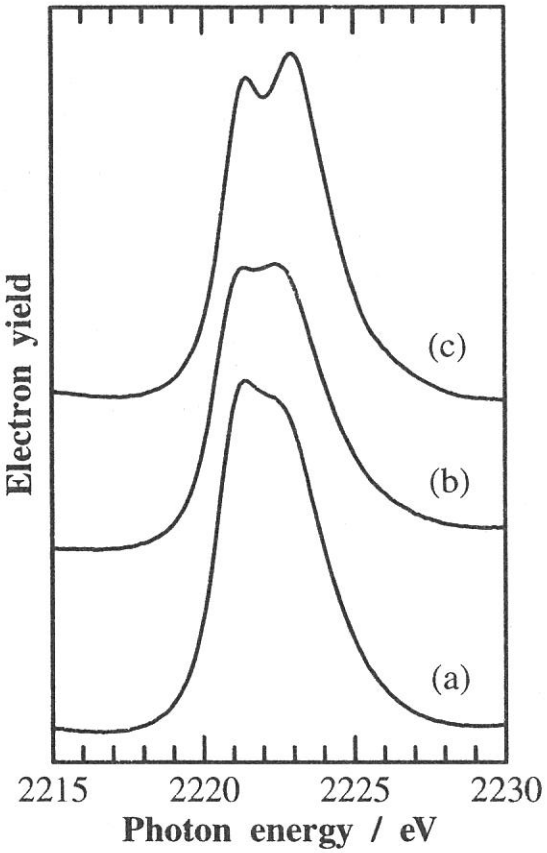

Fig.1 Zr L_3–edge XANES spectra on sulfated ZrO_2 calcined at (a)673K, (b)773K, (c)873K

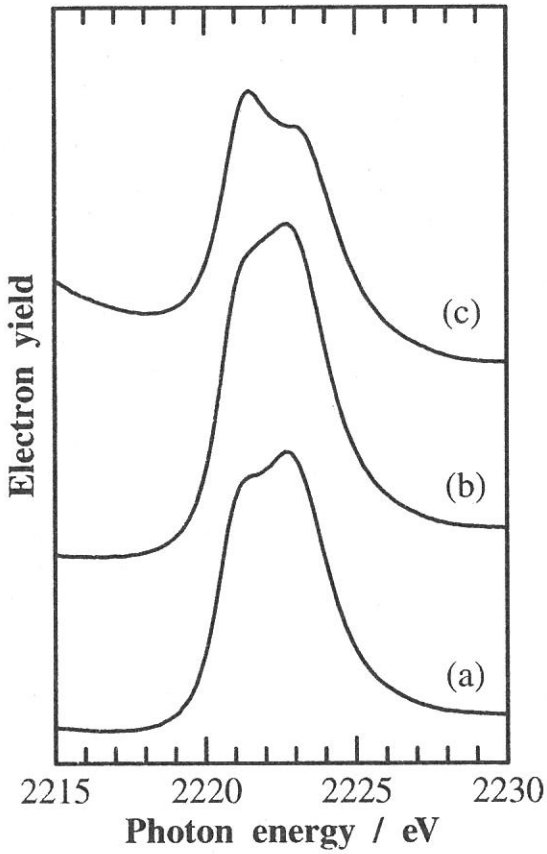

Fig.2 Zr L_3–edge XANES spectra on sulfated Fe/ZrO_2 calcined at (a)673K, (b)773K, (c)873K
Temperature is indicated the secondary calcination temperature.

References

[1] C. Y. Hsu, C. R. Heimbuch, C. T. Armes, and B. C. Gates, *J.Chem.Soc., Chem.Commun.*, 1645(1992).

[2] A. Jatia, C. Chang, J. D. MacLeod, T. Okubo, and M. E. Davis, *Catal.Lett.*, **25**, 21(1994).

[3] M. A. Coelho, D. E. Resasco, E. C. Sikabwe, and R. L. White, *Catal.Lett.*, **32**, 253(1995).

[4] V. Adeeva, J. W. de Haan, J. Jänchen, G. D. Lei, V. Schünemann, L. J. M. van de Ven, W. M. H. Sachtler, and R. A. van Santen, *J.Catal.*, **151**,364(1995).

[5] J. E. Tábora, and R. J. Davis, *J.Chem.Soc. Faraday Trans.*, **91**, 1825(1995)

[6] T. Kosaka, T. Ohnari, Y. Takahashi, and S. Hasegawa, *UVSOR activity report*, 164(1997)

(BL-7A)

Al K-edge XANES Study for the Quantification of Aluminum Coordinations in Alumina

Ken-ichi Shimizu, Yuko Kato, Tomoko Yoshida[A], Hisao Yoshida, Atsushi Satsuma and Tadashi Hattori[B]

Department of Applied Chemistry, Graduate School of Engineering, Nagoya University, Chikusa-ku, Nagoya 464-8603
[A]Center for Integrated Reserch in Science and Engineering, Nagoya University, Chikusa-ku, Nagoya 464-8603
[B]Research Center for Advanced Waste and Emission Management, Nagoya University, Chikusa-ku, Nagoya 464-8603

Transition aluminas, such as γ-Al_2O_3, formed by partial dehydration of aluminum hydrates have been of catalytic importance [1]. However, because of their poor crystallinity, an accurate structure of the transition aluminas is not known except for θ-Al_2O_3, in which Al atoms are equally distributed between tetrahedral and octahedral site of the spinel [2]. Although ^{27}Al MAS NMR can be used to distinguish several Al atoms with different local structures, its application to a quantitative structural analysis of amorphous alumina is difficult [3]. Recently, we reported that Ga atoms with different coordination symmetry can be estimated quantitatively by a deconvolution analysis of Ga K-edge XANES [4]. In this study, the Al K-edge XANES analysis is used to quantitatively determine the tetrahedral and octahedral Al atoms in the transition aluminas.

A series of alumina with various phases were prepared by calcining aluminum hydrate (boehmite) in air at various temperatures (673-1773 K) for 2 h. Mordenite-type aluminosilicate (JRC-Z-HM15, SiO_2/Al_2O_3 =15) containing Al atoms in the zeolite framework was supplied from the Catalysis Society of Japan. θ-Al_2O_3 was prepared by calcining γ-Al_2O_3 (JRC-ALO-4) at 1273 K for 12 h. Crystal phase of these samples was confirmed by X-ray diffraction and was noted in the caption of Fig. 1.

Al K-edge X-ray absorption spectra were measured on BL-7A at UVSOR with a ring energy of 750 MeV and a stored current of 70-220 mA in a mode of total electron yields. An YB_{66} double crystal monochromator was used, and the absolute energy scale was calibrated to a negative glitch due to Y L_3 peak of the YB_{66} at 2080.0 eV [5]. The step with of the monochromater scanning was 0.01° , which corresponds to about 0.3 eV at 1560 eV.

Fig. 1 shows the normalized Al K-edge XANES spectra of alumina samples together with those of some reference compounds of known structure. For the mordenite, which was employed as a model compound of the AlO_4 tetrahedra, a white line feature was appeared at 1566 eV. The sample calcined at 1773 K (α-Al_2O_3, corundum) and boehmite are regarded as model compounds for AlO_6 octahedra. The XANES spectrum of them exhibited a strong white line feature at 1568 eV, together with a broad peak at around 1571-1572 eV. The peaks at 1566 eV and 1568 eV in the spectra exhibited the same energy position as those previously reported for AlO_4 and AlO_6 model compounds, respectively [6], and thus they were assigned to octahedral and tetrahedral Al, respectively. A broad peak at around 1571-1572 eV is known to be due to AlO_6 octahedra [6]. This peak can include multiple scattering contributions [7], and thus it was not employed for the analysis in the present study. For the transition aluminas, which were calcined in the range 673 K to 1273 K, XANES spectra exhibited three distinguishable peaks due to AlO_4 (1566 eV) and AlO_6 (1568 and 1572 eV). It appears that the relative intensity of each peak differs from sample to sample.

To estimate the ratio of Al atoms in tetrahedral and octahedral sites in transition aluminas, the deconvolution analysis of XANES spectra [4] was carried out. Fig. 2 shows the deconvoluted spectrum of θ-Al_2O_3 as an example. The analysis was performed on the assumption that the XANES spectrum is composed of three Gaussian functions for white line peaks due to AlO_4 (1566 eV) and AlO_6 (1568 eV) and the third peak at around 1571-1572 eV and one arctangent function for continuum absorption. Thus, the best parameters, *i.e.*, the exact peak energy, the FMWH and the peak area of each Gaussian were determined so as to simulate the original spectra and were listed in Table 1. The positions of the first and the second Gaussian peaks were centered at 1565.5$\pm$0.1 eV and 1567.7$\pm$0.2 eV, which were almost identical to those of AlO_4 and AlO_6, respectively, within an experimental error. For θ-Al_2O_3, the ratio of the areas of 1566 eV peak and 1568 eV peak was determined to be 50/50, which is in good agreement with the value derived from X-ray diffraction analysis [2]. This suggests that the ratio of AlO_4/AlO_6 in the samples can be estimated quantitatively from the ratio of each Gaussian peak areas.

By using this method, the ratio of AlO_4 and AlO_6 was estimated for a series of transitional aluminas and plotted as a function of calcination temperature (Fig. 3). The result shows that the ratio of AlO_4 and AlO_6 is a function of the calcination temperature. For aluminum hydrate (boehmite), as expected, AlO_6 octahedra are predominant. As calcination temperature increases up to 1073 K, the fraction of AlO_4 increases up to the value of 36 %, and then it decreases at higher calcination temperature. For the sample calcined at 1773 K, which is classified as α-Al_2O_3, AlO_6 octahedra are predominant. Thus, this method is shown to be helpful for a better understanding of the effect calcination conditions on the local structure of the transition aluminas.

In conclusion, the deconvolution analysis of Al K-edge XANES is provided as a novel characterization method for the quantitative analysis of Al coordination states (tetrahedra and octahedra) in aluminum oxides. This method can now be used to determine the coordination states of unknown aluminum oxides.

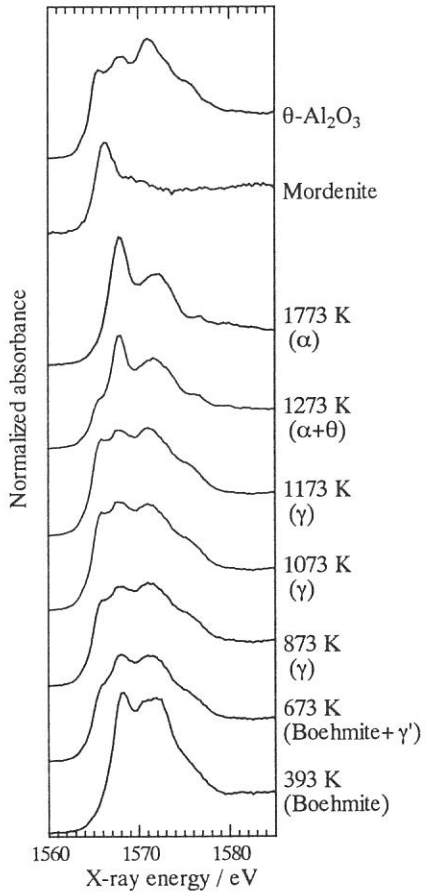

Figure 1 Al K-edge XANES spectra of alumina samples and reference compounds.

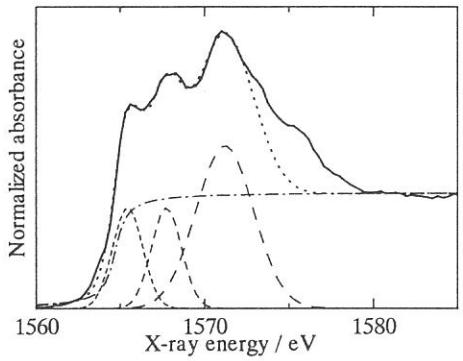

Figure 2 Al K-edge XANES spectrum of θ -Al_2O_3 (-) and the simulated spectrum (・・・), which is composed of three Gaussian (---) and one arctangent (-・-) functions.

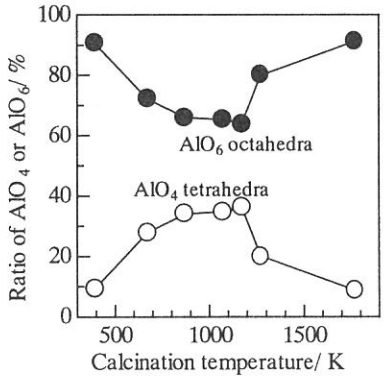

Figure 3 Ratio of AlO_4 tetrahedra (○) and AlO_6 octahedra (●) in alumina samples as a function of calcination temperature.

Table 1: Parameters of deconvoluted peaks in XANES spectra of aluminum oxides.

sample	AlO_4 tetrahedra / eV			AlO_6 octahedra / eV			third peak / eV			
calc. temp./K	position	FWHM	area	position	FWHM	area	position	FWHM	area	AlO_4/AlO_6
θ -Al_2O_3	1565.5	2.1	1.8	1567.8	2.1	1.8	1571.2	4.0	5.6	50/50
393	1565.5	1.8	0.5	1567.9	2.4	5.3	1571.5	5.0	13.5	9/91
673	1565.6	1.7	1.1	1567.7	2.6	2.9	1571.3	5.1	7.5	28/72
873	1565.6	1.7	1.3	1567.6	2.6	2.5	1571.3	5.0	6.3	34/66
1073	1565.6	1.7	1.9	1567.6	2.7	3.5	1571.3	5.1	8.4	35/65
1173	1565.5	1.7	1.9	1567.5	2.7	3.3	1571.2	4.8	7.7	36/64
1273	1565.4	2.0	0.7	1567.8	1.8	2.8	1571.5	5.1	6.1	20/80
1773	1565.4	1.7	0.5	1567.7	2.4	5.3	1571.8	4.4	5.7	9/91

References

[1] H. Knozinger, P. Ratnasamy, *Catal. Rev. Sci. Eng.*, 17 (1978) 31.

[2] R.-S. Zhou, R. L. Snyder, *Acta Cryst.*, B47 (1991) 617.

[3] G. Kunath-Fandrei, T. J. Bastow, J. S. Hall, C. Jager, M.E. Smith, *J. Phys. Chem.*, 99 (1995) 15138.

[4] K. Nishi, K. Shimizu, M. Takamatsu, H. Yoshida, A. Satsuma, T. Tanaka, S. Yoshida, T. Hattori, *J. Phys. Chem. B*, 102 (1998) 10190.

[5] T. Kinoshita, Y. Takata, T. Matsukawa, H. Aritani, S. Matsuo, T. Yamamoto, M. Takahashi, H. Yoshida, T. Yoshida, Y. Ufktepe, K. G. Nath, S. Kimura, Y. Kitajima, *J. Syncrotron Rad.*, 5 (1998) 726.

[6] G.A. Waychunas, G.E. Brown Jr., *EXAFS and Near Edge Structure III*; Springer-Verlag: Berlin, (1984) 336.

[7] D. Li, G.M. Bancroft, M.E. Fleet, X.H Feng, Y. Pan, *American Mineralogist*, 80 (1995) 432.

(BL7A)

Mg K-Edge XANES Study of Forsterite Precursor Prepared from Heterogeneous Alkoxide Solution and Crystallization

Takeshi SHIONO, Takushi MINAGI, Hirofumi ARITANI and Toshihiko NISHIDA

Department of Chemistry and Materials Technology
Kyoto Institute of Technology
Matsugasaki, Sakyo-ku, Kyoto, 606-8585, Japan

1 Introduction

Forsterite, Mg_2SiO_4 has good properties in dielectric loss and electric insulator at high frequency and at high temperatures. However, it is very difficult to prepare dense forsterite with high-purity and stoichiometric composition by a conventional method. Sol-gel method has been extensively studied because of high-purity and good homogeneity, low temperature processing and fabrication. These advantages are suitable for synthesizing fine and high-purity ceramic powder as a starting material. Author et al.[1] prepared forsterite powder with good sinterability from heterogeneous alkoxide solution containing fine MgO successfully. However, the formation mechanism of forsterite was not clarified.

In the present study, the crystallization mechanism from forsterite precursor was investigated through Mg K-edge X-ray near-edge structure (XANES).

2 Experimental

Forsterite precursor was synthesized from tetraethyl-orthosilicate, TEOS and fine MgO powder with mean particle size of 10nm[2]. MgO powder was added to partially hydrolyzed TEOS solution and subsequent addition of water promoted gelation of the solution. The precursor was dried and calcined at a temperature from 400°C to 1000°C in air. The crystalline phase of calcined powder was examined with XRD analysis. The thermal behavior was measured at a heating rate of 5°C by DTA.

Mg K-edge XAFS measurements were carried out on the BL-7A at UVSOR facility in the Institute of the Molecular Science, Okazaki. The spectra were recorded in a total electron yield, using a YB_{66} two-crystal monochromater. Ground samples were spread to carbon film on the first photodynode made of CuBe of the electron multiplier.

3 Results and Discussion

The forsterite precursor was recognized as a small amount of $Mg(OH)_2$ and amorphous phase from XRD analysis. $Mg(OH)_2$ in the precursor was transformed to MgO around 400°C. Forsterite phase was found to form at 800°C. These changes were also observed as endothermic and exothermic reactions, respectively. Figure 1 shows Mg K-edge XANES spectra of forsterite precursor and powders calcined at various temperatures. Figure 2 also shows Mg K-edge XANES spectra of some reference compounds. Spectra of $Mg_2Si_3O_8$ and $MgSiO_3$ in Fig.2 were measured by Yoshida et al.[3]. At the temperature where the formation of MgO was recognized, the rest (amorphous phase) except MgO is inferred to consist of Si rich composition, compared with stoichiometric forsterite (Mg_2SiO_4). From Mg K-edge XANES spectra as shown in Fig.1 and 2, in fact, the local structure of calcined powder is found to be very similar to that of $Mg_2Si_3O_8$. Although this phase is amorphous and the long range order is not recognized by XRD analysis, the structure in short range is judge to be almost the same as that of $Mg_2Si_3O_8$. The exothermic reaction around 800°C would result from the formation of forsterite due to the reaction between

MgO and amorphous $Mg_2Si_3O_8$. In conclusion, the formation of forsterite from the precursor is found to be composed of two step, the transformation from $Mg(OH)_2$ to MgO and the transformation from the reaction between MgO and $Mg_2Si_3O_8$.

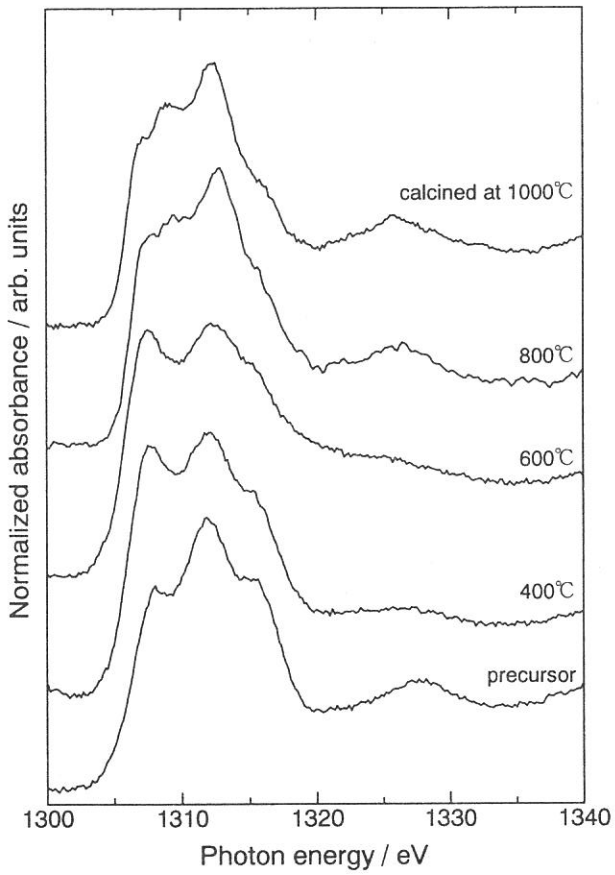

Fig.1.Mg K-edge XANES spectra of forsterite precursor and powders calcined at various temperatures.

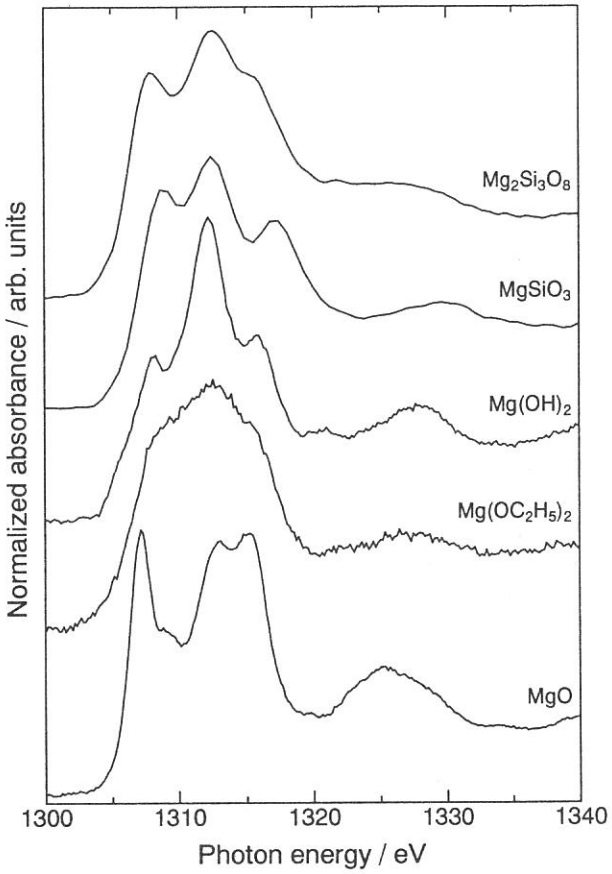

Fig.2.Mg K-edge XANES spectra of reference compounds.

References

1) T.Shiono, K.Miyamoto, Y.Sugishima, Y.Okamoto, K.Hayashi and T.Nishikawa, *J. Powder and Powder Metallurgy*, **41**, (1994) 573-76.

2) T.Shiono, T.Nishida, Y.Okamoto, Y.Sugishima and T.Nishikawa, *Ceramic Transactions : Ceramic Powder Science IV*, **22** (1991) 69-74.

3) H.Yoshida, T.Tanaka, K.Nakatsuka, T.Funabiki and S.Yoshida, *Stud. Surf. Sci. Catal.*, **90** (1994) 473-78.

(BL7A)

Structural study of Al in a series of Aluminosilicate Minerals by X-ray Absorption Spectroscopy.

H. Ichihashi, T. Kurisaki, T. Yamaguchi, T.Yokoyama[1], and H. Wakita*
Department of Chemistry, Faculty of Science, Fukuoka University, Nanakuma, Jonan-ku, Fukuoka 814-0180, Japan
[1]*Department of Chemistry, Faculty of Science, Kyushu University, Hakozaki, Higashi-ku, Fukuoka 812, Japan*

Al *K* X-ray Absorption Near Edge Structure (XANES) spectra of a series of aluminosilicate minerals were measured on the BL7A at the UVSOR of the Institute for Molecular Science, and analyzed by a DV-Xα MO calculation method. The aluminosilicate minerals contain various oxygen coordinated Al(III), e.g. four-, five- and six- (1:1), and six-fold. In this study, the Al *K* XANES spectra of anorthite [$CaAl_2Si_2O_8$], andalusite [Al_2SiO_5] and kaolinite [$Al_2Si_2O_5(OH)_4$] were measured and analyzed in terms of the electron transition probabilities. Their coordination structures and their bond characters were also discussed. The results were compared with those of NMR measurements.

Keywords: Al-K XANES, aluminosilicate, molecular orbital calculation

1. Introduction

The electronic structure aluminosilicate minerals have not been studied in great detail. Recently, X-ray absorption spectroscopy, a powerful tool for structural analysis has been applied for studying the electronic property around the selected atom. Especially, XANES spectra contain the structural information, which is sensitive to the electronic state around the absorbing atom.

In this paper, we measured Al *K* XANES spectra for three aluminosilicate minerals with different Al types (environment) were analyzed by a DV-Xα MO calculation method and assigned the spectral features in terms of electron transition probability. The samples analyzed in this work are a series of aluminosilicalte minerals, anorthite [$CaAl_2Si_2O_8$: four- coordinated], andalusite [Al_2SiO_5 : five- and six-coordinated] and kaolinite [$Al_2Si_2O_5(OH)_4$:six-coordinated].

2. Experiment and calculation

The Al *K* XANES spectra were measured on the BL7A at the UVSOR of the Institute for Molecular Science (Okazaki, Japan), a crystal monochromater beam line with two YB_{66} crystals. The storage ring was operating at electron energy of 750 MeV. All of XANES spectra were measured by total electron yield method.

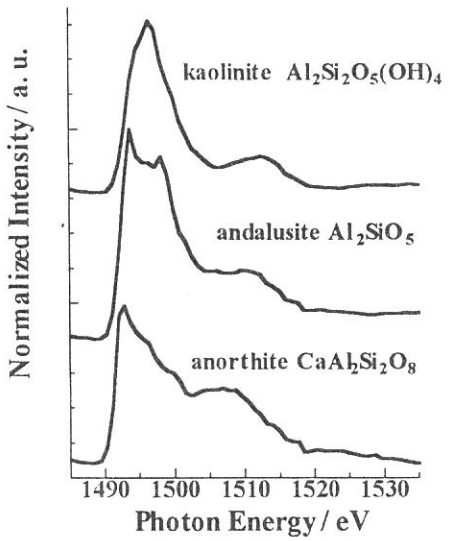

Fig.1 Al *K* XANES spectra of three aluminosilicate minerals

The DV-Xα molecular orbital calculations of these minerals were performed using the default values for well potential values for all atoms, and the transition state method.

3. Results and discussion

Based on the Al *K* XANES spectral measurements of a variety of Al compounds, it was noted that the Al *K* edge shifts to the higher energy side with increasing of the coordination number around the aluminum atom[1),2)]. The Al *K* XANES spectra of aluminosilicate minerals containing Al with various coordination numbers are presented in Fig. 1. Energy shift in our measurements agrees well with the previous measurements. The model clusters for the use of the DV-Xα calculation contain up to the third coordinated shells. Presented in Figs. 2-4 show the measured and the calculated XANES spectra. As seen in these figures, the measured Al *K* XANES spectra agree well with the spectra calculated using the DV-Xα calculations. The Al *K* XANES are resulting from dipole allowed electron transitions from Al 1s orbital to the molecular orbitals mainly consisting of M 3p and M 3d orbitals [: M is a second shell atom.]. As seen in Fig. 1, the measured Al *K* absorption spectrum of andalusite is broader than the Al *K* absorption spectra of the other minerals, probably because andalusite has 5- and 6-coordinated Al, and the

5-coordinated Al in andalusite has a lower symmetry than the other minerals.

The DV-Xα M. O. calculation gives results of net charge and bond overlap population. The relationship between the coordination structure and bond characters for 4-, 5- and 6-coordinated Al can be interpreted from the difference in net charge and bond overlap population of anorthite and andalusite. The effective charge increases with increasing of the coordination number from 4 to 6, and the highest peak position shifts to the higher energy side. Furthermore, with the increases in coordination number of the Al, the Al-O distances in these aluminosilicate minerals increase, indicating that the Al-O bond becomes more ionic characters. By comparing the result of andalusite and kaolinite containing 6-coordinated Al, kaolinite shows lower net charge value than the net charge of andalusite and for the bond overlap population. Because the octahedral Al coordination structure of kaolinite is more distorted than that of andalusite.

The ^{27}Al MAS NMR method is also a powerful tool to probe the coordination structure of Aluminum. Fig. 5 shows the ^{27}Al MAS NMR measurements of three aluminosilicate minerals. These analytical results of Al in the aluminosilicate minerals (anorthite, andalusite[3] and kaolinite) show good agreement with those of ^{27}Al MAS NMR measurements with our previous measurements [4), 5)] for the mullite and mullite precursors. Further, the ^{27}Al MAS NMR chemical shifts of three aluminosilicate minerals, which have 4, 5, and 6 coordinate aluminums, are in good agreement with the corresponding XANES spectral changes.

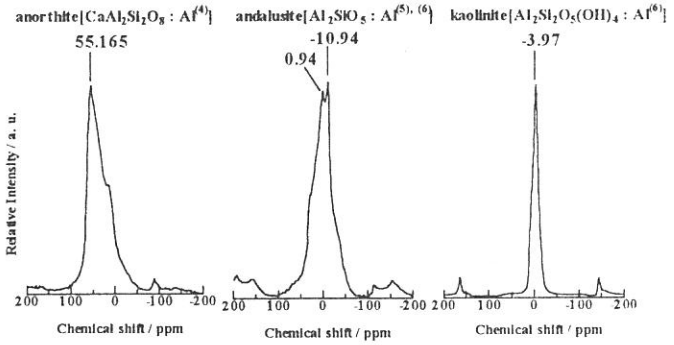

Fig. 5 ^{27}Al MAS NMR spectra of three aluminosilicate minerals. Chemical shift range ; four-fold coordinated Al : 0-30 ppm five-fold coordinated Al : 30-40 ppm six-fold coordinated Al : 40-80 ppm.

4. Conclusions

Al *K* X-ray Absorption Near Edge Structure (XANES) spectra of a series of aluminosilicate minerals were measured on the BL7A at the UVSOR of the Institute for Molecular Science (Okazaki, Japan). The measured spectra are in good agreement with the results from our DV-Xα MO calculations. The ^{27}Al MAS NMR chemical shifts of three aluminosilicate minerals, which have 4, 5 and 6 coordinate aluminums, are in good agreement with the corresponding XANES spectral change.

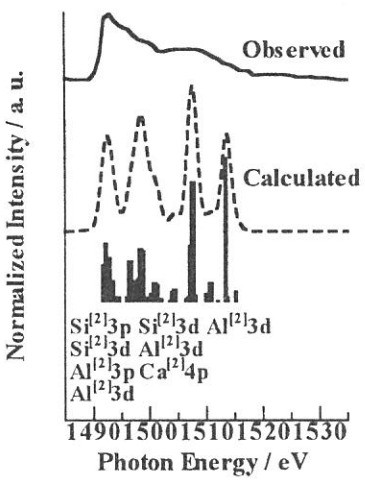

Fig. 2 Observed and calculated Al *K* XANES spectra of anorthite[$CaAl_2Si_2O_8$].

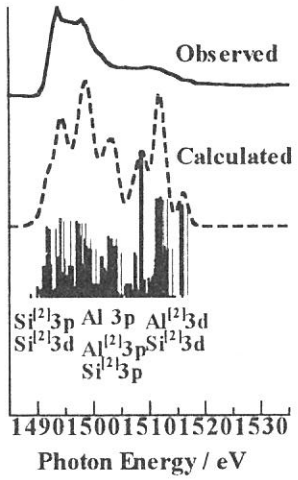

Fig. 3 Observed and calculated Al *K* XANES spectra of andalusite[Al_2SiO_5].

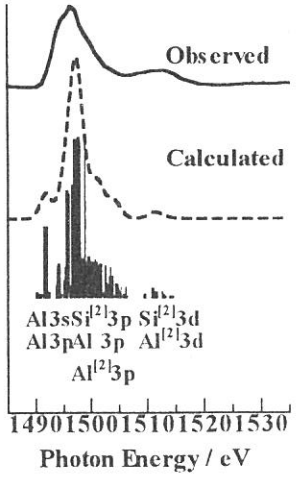

Fig. 4 Observed and calculated Al *K* XANES spectra of kaolinite[$Al_2Si_2O_5(OH)_4$].

References

1) Joe Wong, Z. U. Rek, T. Tanaka, etc., *Physica B* 208&209 220-222 (1995).
2) Joe Wong, G. N. George, etc., *Solid State Communication*, Vol. 92, No. 7, pp559-562 (1994).
3) Lawrence B., Alemany and Garry W. Kirker, *J. Am. Chem. Soc.*, 108, 6158-6162, (1986)
4) Y.Ikeda,T.Yokoyama, S.Yamashita, H.Wakita, Jpn.J.Appl. Pys. Vol32(1993)Suppl. 32-2, pp.670-672.
5) Y.Ikeda, T.Yokoyama, S.Yamashita, T.Watanabe, H.Wakita, Advances in X-ray Chem. Anal. Jpn.,27, 211-219(1995).

(BL-7A)

Influence of Ligands on Cu L XAS Spectra of Copper(II) Compounds

Ken-ichi Shimizu, Hajime Maeshima, Hisao Yoshida, Atsushi Satsuma, and Tadashi Hattori*

Department of Applied Chemistry, Graduate School of Engineering, Nagoya University, Chikusa-ku, Nagoya 464-8603, Japan.
**Research Center for Advanced Waste and Emission Management, Nagoya University, Chikusa-ku, Nagoya 464-8603, Japan.*

Recently, we have reported that Cu L_3 XAS is useful for the quantitative analysis of Cu(II) coordination states (tetrahedra and octahedra) in the copper-aluminate catalysts.[1] However, understanding of the influence of coordination state on XAS spectra is of empirical. We report herein the systematic XAS studies of a series of Cu(II) model compounds. The empirical regularity on the observed chemical shifts is first obtained, and then it is interpreted in terms of a basic crystal-field theory.

The copper(II) compounds studied in the present study were obtained as follows. CuO, $Cu(acac)_2$, $CuBr_2$, $CuCl_2 \cdot 2H_2O$, $Cu(OH)_2$, and phthalocyaninatocopper(II) ($[Cu(C_{32}H_{16}N_8)]$=[Cu(pc)]) were purchased commercially. $CuCl_2$ was obtained by the dehydration of the $CuCl_2 \cdot 2H_2O$. Copper(II) containing mixed oxide of stoichiometric spinel ($CuCr_2O_4$, $CuFe_2O_4$ and $CuAl_2O_4$) and copper aluminate with Cu content of 6 wt.% were prepared by a coprecipitation method [1]. Cu L XAS spectra were measured on BL-7A at UVSOR with a ring energy of 750 MeV and a stored current of 70-220 mA in a mode of total electron yields. A double crystal beryl monochromator was used, and the absolute energy scale was calibrated to the Cu $2p_{3/2}$ peak in CuO at 931.3 eV [2]. The intensity of the spectra have not been normalized because of missing of an adequate normalizing procedure. The electronic absorption spectra were measured using UV-VIS spectrometer (JASCO V-750) in a diffuse reflectance mode.

Figure 1a shows the L_3 XAS spectra of Cu(II) compounds. All the spectra exhibit a large white line feature, which is attributed to the transition from the $2p_{3/2}$ to the lowest unoccupied $3d$ state. The unoccupied 3d level of Cu^{2+} (d^9) compounds exists only at the highest 3d orbital. Thus, one symmetric absorption peak is present except for $CuAl_2O_4$, which contains two kinds of Cu(II) species (60% T_d and 40% O_h) [1]. It appears that the energy position of white line is characteristic to each compounds. Table 1 summarizes the positions of the peak in the order of increase in the energy. For Cu(II) compounds where Cu is octahedrally coordinated to six oxygen atoms, 6wt% Cu-Al_2O_3, $CuFe_2O_4$ and $Cu(OH)_2$, the peak position is 0.5-0.7 eV higher than those of the Cu(II) compounds containing tetrahedral CuO_4, $CuAl_2O_4$ and $CuCr_2O_4$. A further shift of the peak to the higher energy is observed for the compounds with strongly distorted octahedral symmetry and square planer symmetry. Within the compounds of the same symmetry, the peak tends to shift to higher energy with an decrease in the electronegativity of the bonding ligand as reported in an earlier report [3].

Figure 1b shows the Cu L_2 spectra, which exhibit a single $2p_{1/2} \rightarrow 3d$ transition peak. In the same manner as L_3 spectra, the position of the peak is shifted to the higher energies in the order of tetrahedra < octahedra < distorted octahedra < square planner.

On the basis of crystal-field theory, the crystal-field splitting ($10Dq$) increases in the order of tetrahedra < octahedra < distorted octahedra < square planner (spectrochemical-series). It is likely that the order of positive shift of the $2p \rightarrow 3d$ transition peaks corresponds to the crystal-field splitting. Table 1 includes the $10Dq$ value estimated from the d-d transition peak in UV-VIS spectra. By comparison with the XAS data, it is confirmed that the positive shifts in the $2p \rightarrow 3d$ transition peaks are systematically correlated to the increase in the crystal-field splitting. The energy position of these $2p \rightarrow 3d$ transition peaks should correspond to the energy difference between $2p$ level and the highest unoccupied level of the crystal-field, whose energy increases in the same order as $10Dq$. Therefore, it can be concluded that the positive shift in the absorption energies can be attributed primarily to an increase in the highest unoccupied level of the crystal-field, which is due to an increase in the crystal-field splitting.

In summary, the chemical shifts of the $2p \rightarrow 3d$ peaks in the Cu $L_{2,3}$ XAS spectra, which systematically correlated to the change in $10Dq$, was understood in terms of the basic crystal field concept. From the observed relationship, Cu L XAS can now be used to determine the crystal-field data and coordination environments of unknown Cu(II) compounds. Finally, the chemical shift concept obtained in this study will be useful for an improved understanding of X-ray absorption spectra.

References

[1] K. Shimizu, H. Maeshima, H. Yoshida, A. Satsuma, and T. Hattori, *Jpn. J. Appl. Phys.*, in press.
[2] M. Grioni *et al.*, *Phys. Rev. B* 39 (1989) 1541.
[3] A. S. Koster, *Molec. Phys.* 26 (1973) 625.

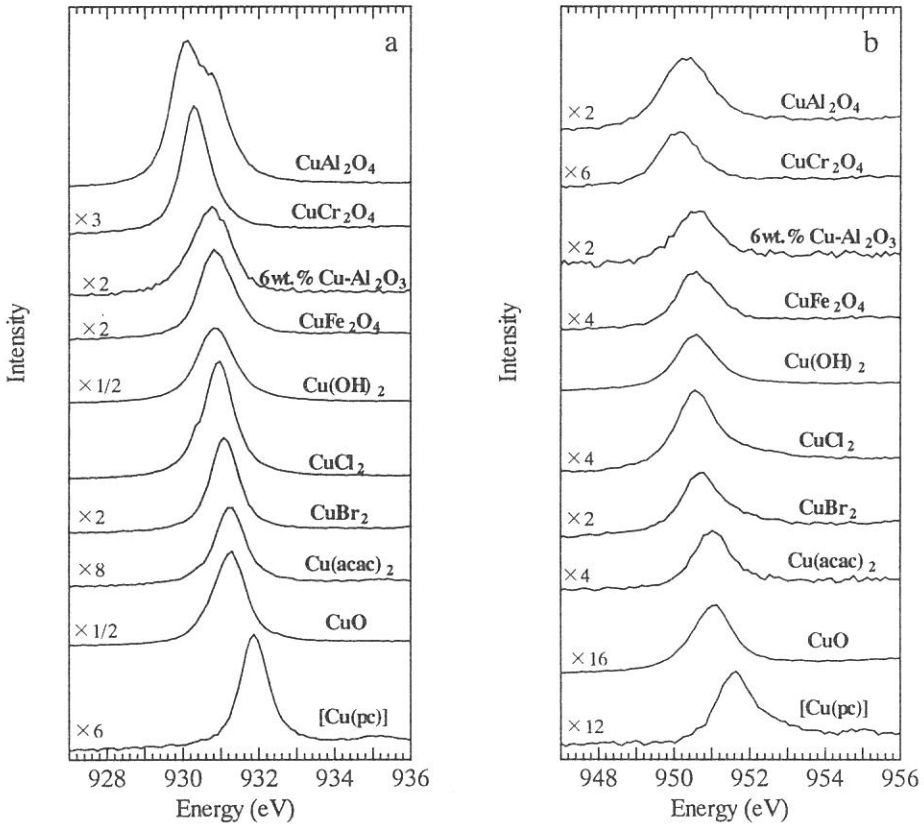

Figure 1. Cu L_3 (a) and L_2 (b) absorption spectra of a series of divalent Cu compounds.

Table 1: Characteristics of Cu $L_{2,3}$ XAS spectra and 10Dq data for Cu(II) compounds.

Sample	Symmetry	$2p_{3/2}\rightarrow 3d$ / eV	$2p_{1/2}\rightarrow 3d$ / eV	$10Dq$[a] / eV
$CuAl_2O_4$	$T_d(O_4)+O_h(O_6)$	930.1	950.3	0.8-0.9
$CuCr_2O_4$	$T_d(O_4$, c/a=0.92[b])	930.3	950.2	1.0-1.1
6wt% Cu-Al_2O_3	$O_h(O_6)$	930.8	950.6	1.5-1.7
$CuFe_2O_4$	$O_h(O_6$, c/a=1.06[b])	930.8	950.6	1.5-1.7
$Cu(OH)_2$	$O_h(O_6$, c/a=1.36[b])	930.8	950.6	1.8
$CuCl_2$	$O_h(Cl_6$, c/a=1.28[b])	931.0	950.6	1.5-1.6
$CuBr_2$	$O_h(Br_6$, c/a=1.33[b])	931.1	950.7	1.5-2.1
$Cu(acac)_2$	$D_{4h}(O_4)$	931.3	951.1	1.9-2.3
CuO	$D_{4h}(O_4)$	931.3	951.1	1.7-2.2
[Cu(pc)]	$D_{4h}(N_4)$	931.9	951.6	2.2-2.3

a) $10Dq$ was estimated from the d-d band of UV-VIS spectra.

b) The value c/a corresponds to the degree of distortion.

(BL7A)

Study on the local structure of hydrotalcite catalysts

Tomoko Yoshida,[a] Hisao Yoshida,[b] Kazuya Yamaguchi,[c] Kohki Ebitani,[c] and Kiyotomi Kaneda[c]

[a] *Center for Integrated Research in Science and Engineering Nagoya University, Nagoya 464-8603*

[b] *Department of Applied Chemistry, School of Engineering, Nagoya University, Nagoya 464-8603*

[c] *Department of Chemical Science and Engineering, Graduate School of Engineering Science, Osaka University, Osaka 560-8531*

Introduction

The catalysis and basic property of hydrotalcite materials depend on the atomic ratio of Mg to Al in positively charged Brucite-like layer (1-3). The Al-Mg mixed oxides obtained by calcination of hydrotalcites also show the basic property which can be controlled by changing the calcination temperature as well as the Mg/Al ratio (4). The difference in the basic properties of these materials should be arisen from the different of the local structure around Mg cations. In the present work, we measured Mg K-edge XAFS of uncalcined and calcined hydrotalcites prepared with a variety of Mg/Al ratio, and analyzed the local structure around Mg ions.

Experimental

A typical example $Mg_6Al_2(OH)_{16}CO_3$ (Mg/Al = 3) was prepared as described elsewhere (2). To obtain the calcined hydrotalcite, it was heated at 673 K for 1.25 h in air. In the present work, the uncalcined and calcined hydrotalcite samples with various atomic ratio of Mg to Al (Mg/Al = 3, 5 and 8) were obtained . The hydrotalcite precursors with Mg/Al ratio were referred to as HT3, HT5, and HT8, and their corresponding calcined samples at 673 K were as cHT3, cHT5 and cHT8 hereinafter.

Soft X-ray absorption experiments were carried out on the beam line 7A at UVSOR, Institute for Molecular Science, Okazaki, Japan, with a ring energy 750 MeV and stored current of 80-200 mA. Mg K-edge X-ray absorption spectra were recorded using a beryl two-crystal monochromater. Data were collected in a total electron yield mode under high vacuum ($<10^{-7}$ Torr) at room temperature. The samples were put on the first photocathode made of Cu-Be of the electron multiplier by using adhesive carbon tape.

The curve-fitting analysis was performed for the Fourier-filtered EXAFS with the empirical parameters extracted from EXAFS of MgO calcined at 673 K.

Results and Discussion

Fig. 1 shows Mg K-edge XANES spectra of uncalcined hydrotalcite samples and $Mg(OH)_2$. The main features of the spectra were resemble, indicating that the local symmetry around Mg atoms in hydrotalcite samples was dominantly the same as $Mg(OH)_2$ phase. It is known that Mg ions are surrounded by six OH groups in the Brucite layer of hydrotalcites, and which was confirmed by these spectra. A detailed comparison of the XANES spectra led us to notice the slight difference between the spectra of uncalcined hydrotalcite samples and that of $Mg(OH)_2$, i.e., the peaks at 1305-1320 eV became broad by increasing Al content. This result supported that the incorporation of Al ions with Mg ions occurred over wide range of Mg/Al ratio in hydrotalcite (1) and indicated that the local structure around Mg ion was changed by the substitution of Al ions.

Fig. 2 shows Mg K-edge XANES spectra of hydrotalcites and MgO which were calcined at 673 K. In each spectrum of calcined hydrotalcite, the energy positions of the prominent peaks were the same as those for MgO, indicating that the dehydration of $Mg(OH)_2$ phase in hydrotalcites occurred during heat treatment and MgO phase was produced. However, it is noteworthy that the peak broadening around 1310 eV were observed for the XANES spectrum of cHT3. The XANES spectrum of cHT3 was indicative of the presence of different local structures other than MgO.

To elucidate this, Mg K-edge EXAFS spectra of the calcined samples were further analyzed. The overall patterns of EXAFS oscillations of the calcined samples were similar to that of MgO, although the amplitude became smaller with an increase of the Al content.

The radial structural functions (RSF, in Fig. 3) obtained from these EXAFS showed some differences. The peak appearing around 1.5 Å was assigned to the adjacent oxygen atoms to Mg ions, and the peak around 2.6 Å showed the presence of the second neighboring metal atoms. The magnitude of the peak around 1.5 Å was almost constant, while the peak position for the calcined samples shifted slightly to the shorter distance compared with that of MgO. Moreover, the magnitude of the peak around 2.6 Å was remarkably suppressed as the increase of Al composition.

Here, we performed curve-fitting analysis by using the parameters of Mg-O and Mg-Mg shells by the least-squares method. The results were summarized in Table 1. The interatomic distance of Mg-O in the calcined samples was evaluated to be slightly shorter than that of MgO. As for the second neighboring atoms around Mg in calcined samples, good fitting was obtained by use of one Mg-Mg shell for cHT8 sample, and the interatomic distance was estimated as 2.97 Å, which was the same value as Mg-Mg distance in MgO. On the other hand, the curve fitting was not completed with one Mg-Mg shell for cHT3, *i.e.*, the additional Mg-Mg bond with longer distance than 2.97 Å were required. These curve-fitting results clearly indicate that the interatomic distance between Mg and second neighboring metal atoms became variant by increasing the Al content. That is, the structure of MgO phase in the calcined samples of high Al content was clarified to be disordered due to the substitution of Al for Mg ions.

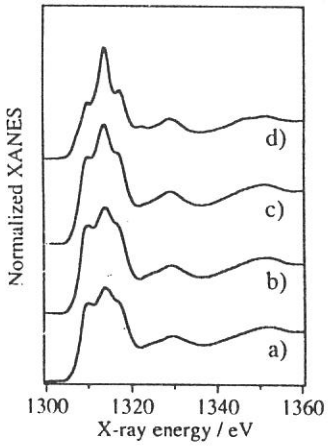

Fig.1 Mg K-edge normalized XANES spectra of a) HT3, b) HT5, c) HT8 and d) $Mg(OH)_2$.

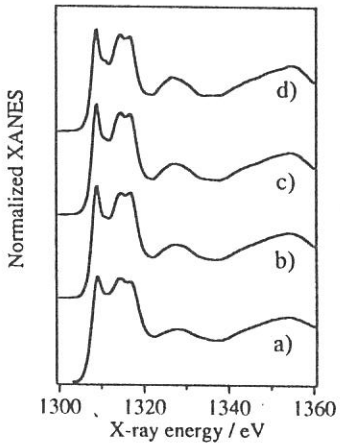

Fig.2 Mg K-edge normalized XANES spectra of a) cHT3, b) cHT5, c) cHT8 and d) MgO calcined at 673 K.

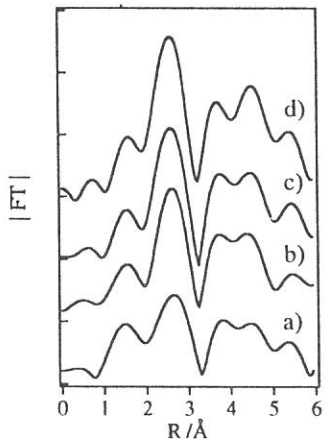

Fig.3 Fourier transforms of k^3-weighted Mg K-edge EXAFS spectra of a) cHT3, b) cHT5, c) cHT8 and d) MgO calcined at 673 K.

Table 1
Results of curve-fitting analyses.

Sample	shell	CN	R / Å	$\Delta\sigma^{2\,a)}$ / Å^2	RF $^{b)}$/%
MgO$^{c)}$	Mg-O	6.0	2.10	0	
	Mg-Mg	12.0	2.97	0	
cHT8	Mg-O	5.8	2.09	0.00199	
	Mg-Mg	11.0	2.97	0.00200	6.5
cHT5	Mg-O	5.7	2.09	0.00311	
	Mg-Mg	10.7	2.97	0.00378	4.2
cHT3	Mg-O	4.9	2.07	0.00395	
	Mg-Mg	7.5	2.98	0.00325	
	Mg-Mg	2.0	3.12	0.00062	4.5

The region of 1.0-3.4 Å in Fig. 4 were inversely Fourier transformed.
The errors in CN and R are ± 10% and ± 0.02 Å, respectively.
a) $\Delta\sigma^2$ is the difference between the Debye-Waller factors of the sample and the reference sample MgO.
b) $RF = [\,(\Sigma\,(\chi(k) - \chi_{calc}(k))^2\,) / (\Sigma\,\chi_{calc}(k))^2\,]^{1/2}$
c) Mg-O and Mg-Mg shells were extracted from EXAFS of MgO.
CN: coordination number, R: interatomic distance

References

1) Cavani, F., Trifiro, F. and Vaccani, A., *Catal. Today*, **11** (1991) 173.
2) Kaneda, K., Ueno, S. and Imanaka, T., *J. Chem. Soc., Chem. Commun.* (1994) 797.
3) Ueno, S., Yamaguchi, K., Yoshida, K., Ebitani, K. and Kaneda, K. *Chem. Commun* (1998) 295.
4) Corma, A, Forn, V. and Rey, F, *J. Catal.* **148** (1994) 205.

(BL-7A)

Mg K-edge XANES Study of Li- and Mn- promoted MgO

Hirofumi Aritani,* Hiroyuki Yamada,* Takashi Nishio,* and Seiichiro Imamura,*
Sadao Hasegawa** and Tsunehiro Tanaka***

**Faculty of Engineering and Design, Kyoto Institute of Technology, Sakyo-ku, Kyoto 606-0962, Japan*
***Department of Chemistry, Tokyo Gakugei University, Koganei, Tokyo 184-8501, Japan*
****Division of Molecular Engineering, Graduate School of Engineering, Kyoto University, Sakyo-ku, Kyoto 606-8501, Japan*

Li-promoted MgO catalyst has been used and applied widely as a selective oxidation of alkanes. In particular, Li-MgO catalysts for oxidative coupling of methane (OCM) reaction have been studied by many workers in 1980s[1-3] because of high reactivity and C_{2+} selectivity. In addition, it is reported that Mn-based catalysts such as Li-Mn-MgO also effective for methane activation.[4,5] Catalytic active species of Li-MgO is recognized as unique oxygen-anion species which were characterized by means of ESR mainly. As for Li-MgO, Li^+-O^- centers which is in equilibrium with surface O^- centers via hole transport were responsible for activation of CH_4.[6] However, different oxygen-species such as O_2^- or O_2^{2-} are proposed as active centers on other OCM catalysts. Consistent active species for OCM reaction have not been decided. In fact, it would be difficult to characterize the active oxygen species in the reaction condition. On the other hand, it is accepted widely that vacant-hole sites such as F-center are generated onto MgO not only in the surface but in the bulk phase by promotion of Li^+ ions. Thus, the characterization of Li-promoted MgO is important for solving the generation of vacancy sites in the bulk phase. But direct observation of vacancy sites in MgO is difficult by means of several spectroscopic study. ESR study is only available for characterization of ESR-active oxygen anions. Although XRD study is available for characterizing the bulk phase on Li-MgO, cristallinity of MgO can only be evaluated. More information about the defect on Li-MgO is looking for. In this study, we applied the Mg K-edge XANES spectra for characterization of the local structure around Mg^{2+} ions of Li-MgO and Mn-MgO. For XANES measurement, total electron-yield mode is used in this study. In this method, a penetration range of XANES is less than 38 nm because a component of electron-yield is mainly low energy secondary electrons.[7,8] The structural information by XANES is reflected in "near-surface region". To compare between XANES and XRD results, the formation of vacancy sites and cristallinity of MgO can be discussed in both surface region and bulk phase.

A MgO sample was obtained by calcination of $Mg(OH)_2$ (Kojundo-Kagaku Kenkyusho Co.) at 873K for 3 h, and followed by cooling at ambient temperature for overnight. Li- or Mn-promoted MgO samples were obtained by impregnation of $Mg(OH)_2$ with aqueous solution of $LiNO_3$ or $Mn(NO_3)_2 \cdot 6H_2O$ (Nacalai Tesque Co.) at 343 K, and then evaporated excess water at 343K to form a paste. Then the paste was dried at 353 K for overnight and calcined at 873 K for 3 h. The Mg K-edge XANES spectra were collected on a facility of BL-7A station of soft X-ray beam line at UVSOR, in the Institute for Molecular Science, Okazaki, Japan, with 750 MeV of a ring energy and 120 - 220 mA of stored current. Each sample was mounted on a carbon-tape, and then attached on a beryllium-copper dynode which was set to the first-stage of electron multiplier placed into a vacuum chamber. After the chamber had been evacuated ($< 2.0 \cdot 10^{-7}$ Torr), the spectrum was recorded in a total electron yield mode at room temperature, using a beryl two-crystal monochromator ($2d$ = 1.5965 nm). The photon energy was calibrated by using Al metal-foil sample at Al K-edge (1559 eV).

Fig. 1 shows the XANES spectra of Li- and Mn- promoted MgO. In case of Li-MgO, the spectra in the range of 5.0 - 15.0 wt% loading reflect MgO-like structure mainly, indicating that cubic structure around Mg exists in the surface region. On the other hand, the spectrum in 2.5 wt%-Li includes another component (deconvoluted curve is shown in Fig 1, in right-bottom hand). It is different from $Mg(OH)_2$ or $Mg_2CO_3(OH)_2$, and rather similar to MgO. This result possibly indicates that MgO-like cubic structure with different Mg-O bonds from that of bulk MgO coexists in near-surface region. It suggests the generation of oxygen-vacancy sites such as F-center and/or substitution of Li^+ ions onto MgO cubic structure. From XRD results, a cristallinity of MgO cubic structure increased by Li promotion until 7.5 wt% loading. At high Li concentration, the vacancy sites may decreased because rich Li^+ cation gives little interaction for MgO. Thus, the vacancy sites generated in low Li concentration, which is localized in near-surface, may relates to the active species for OCM. The phenomenon mentioned above was also seen in case of Mn-MgO. In the region between 2.5 and 15.0 wt% of Mn loading, coexistence of MgO and another cubic structure was observed. At 25.0 wt% Mn loading, almost MgO cubic structure was seen. It suggests that substitutional existence of Mn ions onto MgO cubic structure was occurred because cristallinity of MgO was almost similarly in the whole Mn-MgO samples. In case of Ni-promoted MgO, the phenomenon mentioned above was not observed, as reported.[9] The reason of the difference between Mn-MgO and Ni-MgO has been studying now.

(1) Lee, J. S.; Oyama, S. T. *Catal. Rev. -Sci. Eng.* 1988, 30, 249. (2) Amenomiya, Y.; Birss, V. I.; Goledzinowski, M.; Galuskzka, J.; Sanger, A. R. *Catal. Rev. -Sci. Eng.* 1990, 32, 163. (3) Ito, T.; Lunsford, J. H. *Nature* 1985, 314, 721. (4) Keller, G. E., Bhasin, M. M. *J. Catal.* 1982, 73, 9. (5) Larkins, F. P., Nordin, M. R., *J. Catal.* 1991, 130,147. (6) Driscoll, D. J.; Lunsford, J. H. *J. Phys. Chem.* 1983, 87, 301. (7) Elam, W. T.; Kirkland, J. P.; Neiser, R. A.; Wolf, P. D. *Phys. Rev. B* 1995, 37, 2450. (8) Erbil, A.; Cargill III, G. S.; Frahm, R.; Boehme, R. F. *Phys. Rev. B* 1988, 37, 2450. (9) Yoshida, T.; Tanaka, T.; Yoshida, H.; Funabiki, T.; Yoshida, S.; Murata, T. *J. Phys. Chem.* 1995, 99, 10890.

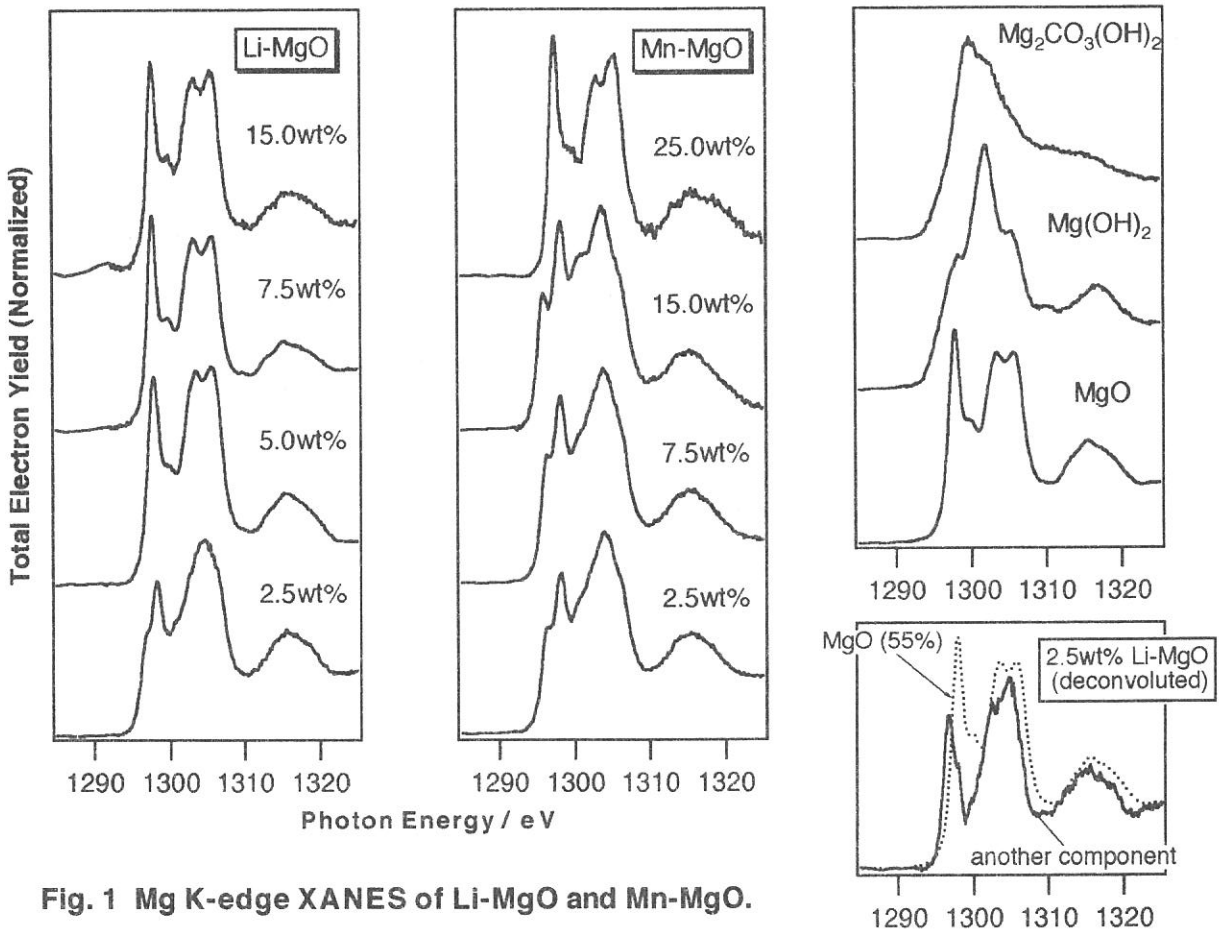

Fig. 1 Mg K-edge XANES of Li-MgO and Mn-MgO.

(BL7A)

Local structure around P atoms in the Ni-P plating films from total electron yield XAFS

Takashi WATANABE, Hisanobu WAKITA*, Tsutomu KURISAKI*, Shuji MATSUO*,
Hikoshiro ICHIHASHI* and Norimasa UMESAKI**
Division of Molecular Science, the Graduate School of Science and Technology, Kobe University, Nada-Ku, Kobe 657-8501, Japan
**Department of Chemistry, Fukuoka University, Jonan-Ku, Fukuoka 814-0180, Japan*
***Department of Optical Materials, Osaka National Research Institute(ONRI), AIST, Ikeda, Osaka 563-8577, Japan*

Introduction

The Ni-P plating film is using for titanium alloys of parts for industrial, automobile, and medical material parts by the purpose of corrosion resistance and the wear resistance improvement. In case of the deposition of the Ni-P plating film, it is important in the control of the physical properties of the film to analyse the deposition mechanism of intermetallic compound Ni_3P by the difference of the deposition processes.[1] By the analysis of XRD , we have confirmed that the Ni-P films obtained at as deposited-200℃ are amorphous, those obtained at 250-300℃forms form intermetallic compound Ni_3P, and those obtained at over 300℃ form crystalline Ni and the precipitate of Ni_3P.

The purpose of this report is to clarify the deposition mechanism of Ni_3P from electroplating and electroless plating Ni-P films under various heating conditions by the use of total electron yield XAFS method and the spectral simulation technique.(Cerius[2], EXCURV92)

Experimental

The samples are those unheated of the deposition electroplating and electroless plating Ni-P films and those heated at 200℃, 250℃, 300℃, 350℃ and 400℃. The film thickness of all samples is 15 μ m. The P *K*-edge XAFS data were collected on a facility of BL-7A station of soft X-ray beam line at UV-SOR. Each sample was prepared for measurement by putting on a beryllium-copper photo dinode which was attached to a first position of the secondary electron multiplier with a carbon tape. After the chamber had been evacuated ($<1.0\times10^{-7}$ Torr), the spectrum was recorded in a total electron yild XAFS method at room temperature, using InSb(111) double crystal monochromater. The XAFS analysis was applied to the obtained P *K*-edge spectrum, and P surroundings was analyzed the local structure and the electronic state. In addition, the result of the spectral simulation which used EXCURV92 with Cerius[2] was compared and examined with the experimental results.

Results and Discussion

As seen in Fig.1, the transition peak from *1s* state of the ground state of P to hybrid orbital state *3p/3d-4s-4p* is observed in P *K*-edge XANES spectra. The positions of A and B correspond to $1s\rightarrow\pi^*$ and $1s\rightarrow\sigma^*$, respectively. The peak of $1s\rightarrow\sigma^*$ becomes clearly as the heat treatment proceeds. Figure 3 shows the simulated radial distribution function (RDF) of P atom surroundings which is calculated from the tetragonal model of Ni_3P seen in Fig.2 and the RDF obtained from the experimental EXAFS signal $k^3\chi(k)$. Figure 3 indicates that the experimental RDF becomes to be similar to the simulated RDF from Ni_3P as the heat-treating temperature increases. The interatomic distances of P-Ni bond does not change into this with 2.28Å among local structural parameters obtained from least square fitting of the experimental value and the theoretical value concerning RDF 1st peak as listed in Table 1. It is supported from approaching by the coordination number of the first neighboring atoms of P advance to coordination number 9 of the first neighboring atoms Ni of P in Ni_3P as the heat-treating temperature increases.

These results give the conclusion that evenif as deposited samples, both of electroless plating and electroplating Ni-P films, are in the forms of quasi-compounds or crystallites of Ni_3P structure in Ni-P plating films. And the samples obtained from the heat treatment are in the forms of larger crystal grain of Ni_3P structure.

Table 1 Local structure parameters obtained from least-square fitting of the experimental value and Theoretical value concerning RDF 1st peak.

Samples		1st neiboring atom	interatomic distance(Å)	coordination number
Electroless plating Ni-P films	As depo.	Ni	2.28	7.9
	250℃, 2hr	Ni	2.28	7.9
	350℃, 2hr	Ni	2.28	8.9
	400℃, 2hr	Ni	2.28	9.0
Electroplating Ni-P films	As depo.	Ni	2.28	7.8
	250℃, 2hr	Ni	2.28	8.7
	350℃, 2hr	Ni	2.28	8.9
	400℃, 2hr	Ni	2.28	9.0

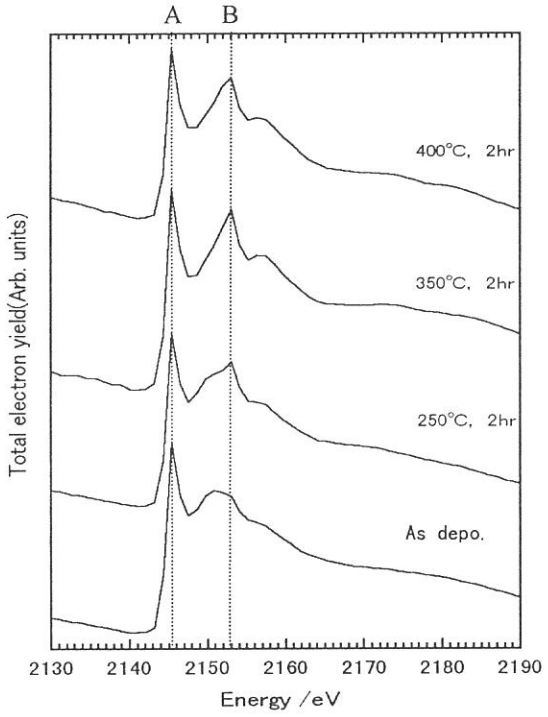

Fig.1. XANES spectra for P K-edge of electroless Ni-P films

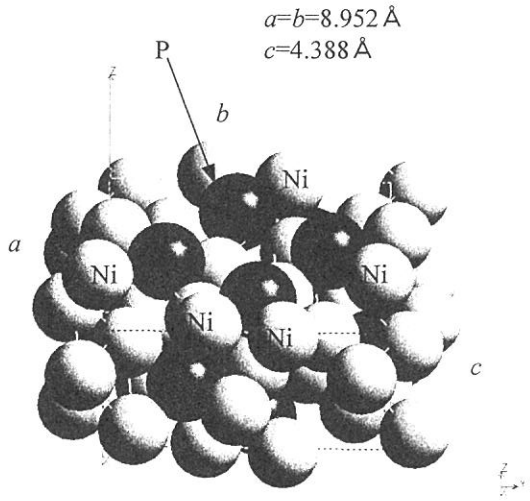

Fig.2. Tetragonal crystal structure of Ni_3P

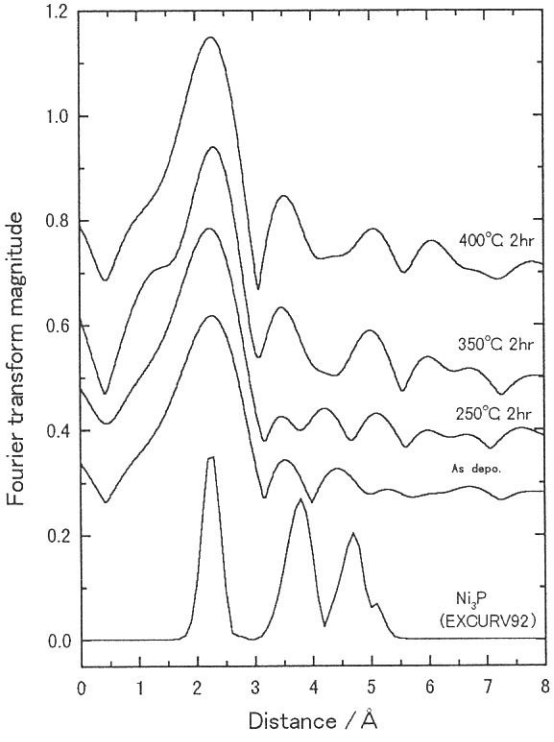

Fig.3. RDF around the P atom ofelectroless plating Ni-P films.

Reference
1) T.Nakayama, Y. Wada, H.Ido, "R&D" Kobe Steel Engineering Reports, **Vol.43**, **No.3**(1993)71.

(BL7A)

Si K-edge XANES Study of Neutron Irradiated Silica Glasses

Tomoko Yoshida[A], Hisao Yoshida[B], Mikio Sakai[C], Takanobu Hara[C] and Tetsuo Tanabe

[A]*Center for Integrated Research in Science and Engineering, Nagoya University, Furo-cho, Chikusa-ku, Nagoya 464-8603*

[B]*Department of Applied Chemistry, School of Engineering, Nagoya University, Furo-cho, Chikusa-ku, Nagoya 464-8603*

[C]*Department of Nuclear Engineering, Graduate School of Engineering, Nagoya University, Furo-cho, Chikusa-ku, Nagoya 464-8603*

Introduction

Radiation effects of high energy particles on silica are one of the main concerns for their application as optical windows, insulators and optical fibers in nuclear environments. Defects in silica such as oxygen vacancy related ones and Si precipitates produced by energetic particles injection have been extensively studied mainly by optical techniques. Recently, it has been also revealed that such defects formation closely relates to electron excitation as well as lattice displacement under radiation.(1-3) However, it has been very difficult to observe directly the electronic and atomic structures of the defects due to their materials characters as amorphous and insulators which do not allow to use diffraction and electron probe techniques. In the present study, we applied X-ray absorption technique to observe the electronic state and the local structure of neutron irradiated silica glasses.

Experimental

Samples used were SiO_2 glasses of 15 mm diameter and 2 mm thickness produced by Toshiba Ceramics, Japan.

Neutron irradiation experiments were carried out at the nuclear reactor YAYOI at the University of Tokyo. During the experiments, YAYOI was operated with a power of 2 kW with an average neutron energy of 1.3 MeV. The fluence of neutron was 3.6×10^{15} n/cm^2.

X-ray absorption experiments were carried out on the beam line 7A at UVSOR, Institute for Molecular Science, Okazaki, Japan with a ring energy 750 MeV and stored current 80-200 mA. Spectra were recorded at room temperature in a total electron yield mode, using a two-crystal InSb monochromator. The sample was put on the first photocathode made of Cu-Be of the electron multiplier.

Results and Discussion

Fig.1 compares Si K-edge XANES spectra of a neutron irradiated silica with that of an unirradiated one. The XANES spectrum of the unirradiated silica sample showed a sharp and prominent peak at around 8 eV (relative to Si K-edge of pure silicon; 1838 eV). This absorption is assigned to atomic-like Si 1s to 3p transition.(4) In silica, a silicon atom occupies at a center of the regular tetrahedron of oxygen atoms. Therefore, Si 3p orbitals must be degenerated resulting in such a sharp absorption. The XANES spectrum of the neutron irradiated silica sample(b) was almost the same as that of the unirradiated one(a), indicating that SiO_4 structures around Si atoms are fundamentally maintained after irradiation. Because the neutron fluence was so small to produce heavy damages such as introduced by He^+ irradiation. Nevertheless, the main peak height was a little lower than that of the unirradiated one. Accordingly, as shown in Fig. 2, Radial structure functions (RSFs) which were obtained by Fourier transforms of k^3-weighted EXAFS spectra, exhibited a certain structural change. In RSFs, the first peaks appearing at around 1.5 Å are attributed to neighboring oxygen atoms (Si-O). By neutron irradiation, the intensity of the first peak was reduced without changing its FWHM (the full width at half maximum). This indicates the decrease in the coordination number of oxygen atoms due to the break of Si-O bonds or the formation of oxygen vacancies. In addition, the peaks at 2-3 Å in RSFs which are ascribed to Si atoms bridged by oxygen (Si-O-Si) became small and slightly

shifted to short distance. This also confirms the existence of oxygen vacancy resulting in shorter Si-Si distance with changing the angle of Si-O-Si. Thus, XAFS should clearly reflect the structural change around Si atoms resulting from oxygen-vacancy formation.

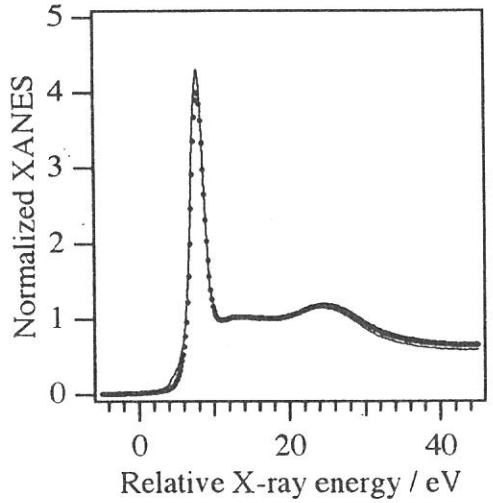

Fig. 1 Si K-edge normalized XANES spectra of a) an uniradiated silica glass (solid line) and b) its neutron irradiated sample (dashed line).

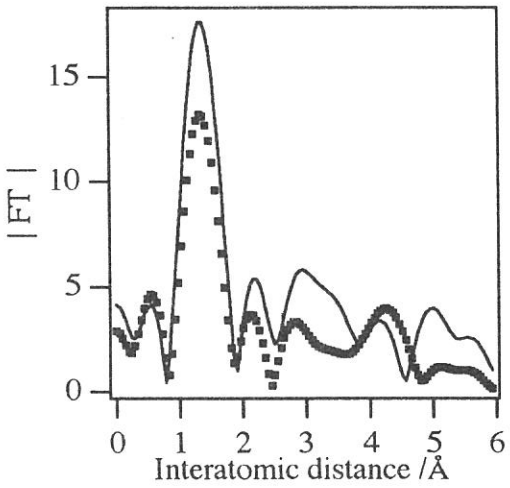

Fig. 2 RSFs obtained by Fourier transforms of k^3-weighted Si K-edge EXAFS of a) an irradiated silica glass (solid line) and b) its neutron irradiated sample (dashed line).

References

(1) M. Fujiwara, T. Tanabe, H. Miyamaru and K. Miyazaki, Nucl. Instr. and Meth. B, 116 (1996) 536.

(2) T. Tanabe, S. Tanaka, K. Yamaguchi, N. Otsuki, T. Iida and M. Yamawaki, J. Nucl. Mater., 212-215 (1994) 1050.

(3) T. Tanabe, M. Fujiwara, T. Iida, S. Tanaka, K. Yamaguchi and M. Yamawaki, Fusion Eng. Design 29 (1995) 435.

(4) T. Tanaka, S. Yoshida, R. Kanai, T. Shishido, H. Hattori, Y. Takata and K. Kosugi, J. Phys. IV France, 7 (1997) 913.

(BL7A)

X-ray Spectrum Measurement in the Range of keV by Ionization Chamber with Divided Electrodes

Tetsunori Taninaka, Masazumi Ishida, *Hironobu Matsuo, *Masayuki Fukao
Graduate School of Science and Engineering, Shizuoka Univ.
**Dept. of Electrical and Electronic Eng. Shizuoka Univ.*
Jouhoku 3-5-1 Hamamatsu 432-8561, Japan

Purpose

The purpose of experiment is to calibrate an Ionization Chamber with Divided Electrodes (ICDE) in the keV range by the monochromatic X-ray generated with 2 crystal spectroscopes of BL7A.

Items to be checked are ; (1)absolute sensitivity, (2)influences of other reactions besides photoelectric effect, (3)photoelectron crossing current among divided electrodes, (4)recombination effects of photoelectrons, and (5)distortion of photoelectron current distribution near photon entrance window.

Principle of Measurement

In the range of keV, the photoelectric reaction is dominant between photons and atoms[1], that is, an incident photon gives the energy to an electron by a single reaction. Therefore, by measuring the spatial distribution of photoelectrons along incident photon path in gas, the incident photon energy spectra can be estimated, since the photon mean free path is known as a function of the energy. The spatial distribution of photoelectrons can be obtained by measuring the current to electron collecting electrodes divided along the photon path. It must be considered that the photoelectrons have enough energy to ionize many gas molecules.

The constructed detector is shown in Fig.1[2]. In a metal cylinder case of 60 mm in dia. and 320 mm long, a pair of parallel plate electrodes are set in axial direction. While one side is of a piece, the other side consists of 4 pieces of 10, 20, 50 and 200 mm wide from the X-ray entrance window. The perpendicular width is 30 mm. The interval of electrode is 25 mm. Adjacent electrodes are separated by 2 mm gap. A thin cylinder is attached inside of and insulated by a thin film from the grounded cylindrical case. The common electrode and the inner cylinder are kept at -500 V. The divided 4 electrodes are connected to negative inputs of Op.Amps. with low input drift current and kept at the virtual ground potential, respectively. To minimize a distortion of electric field near the X-ray entrance window, the wall near the entrance hole is kept at -250 V. The Op.Amps. are installed inside of the cylinder and the output signals are extracted via feedthrough to a data acquisition system. The inside of chamber is kept in 1 atm. air. The X-ray entrance is of 6 mm in dia. and sealed with 4 μm polypropylene film. A swelling of the film due to the atmospheric pressure, which would change in size with temperature and pressurization cycle, made the boundary of sensing area ambiguous. It was improved by supporting the film with stainless steel mesh at the sacrifice of reduced photon flux. The current I_i into the i-th electrode is expressed as

$$I_i = \int_0^{E_a} \left(\exp(-z_{i-1}/\lambda(E)) - \exp(-z_i/\lambda(E))\right) \frac{E}{W} T(E) S(E)\, dE ,$$

where $S(E)$ is photon spectrum, E_a the maximum energy, $T(E)$ the transmission rate of the window film, z_i the distance from the entrance window to the far side boundary of the i-th electrode, W effective ionization energy. The E/W gives the number of electrons which are secondarily produced by a fast electron due to photoionization.

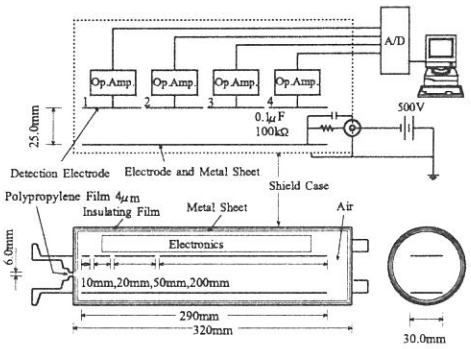

Fig.1 Ionization chamber with divided electrodes

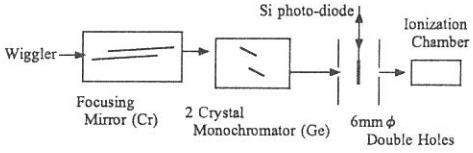

Fig.2 Experimental configuration

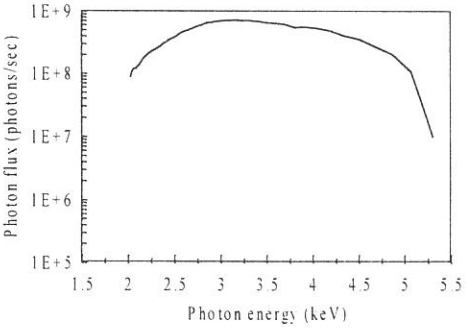

Fig.3 X-ray spectrum (beam current : 100 mA)

Experiment Results

The experimental configuration is shown in Fig.2[3)4)]. A pair of germanium crystals were used for monochromator. The X-ray was introduced through double holes of 6 mmϕ each and 300 mm spacing, into the ICDE. The double holes are set against accidents such as the entrance film damage. Photon flux is measured by a Si photo-diode put between 2 holes as shown in Fig.2. The photon energy vs. flux measured by the Si photo-diode is shown in Fig.3. The flat photon flux was observed over 10^8 photons/sec from 2 keV to 5 keV. The ICDE was calibrated by 0.2 keV step in the whole energy range. Photon energy vs. currents into the four electrodes are shown in Fig.4(a), where the currents are normalized for 1×10^9 photon flux by using spectral curve shown in Fig.3. Theoretically expected curves are shown in Fig.4(b). Although each curve resembles other, there are some discrepancies. The experimental and the theoretical electrode currents normalized by the first electrode one are shown in Fig.5(a) and (b), respectively. Each curve agrees well with other.

The discrepancies observed between Fig.4(a) and (b) are considered to be owing to a shift of photon beam axis on rotating the double crystals to sweep energy. The spectrum of Fig.3 was observed in the middle of two holes, while the ICDE accepted the photons passing through the two holes. A small shift of position and/or angle of the beam axis would bring about serious changes in the energy spectra.

It would be concluded from this experiment about the items to be checked:

(1) Absolute measurement could not be confirmed because of the lack of photon profile in the cross section of photon beam and the beam axis shift on sweeping energy. The ICDE might be used for an absolute measurement from the simplicity of the principle.

(2)-(5) Since the experimentally observed current ratios are well fitted to the theoretical expectations which take account only of photoelectric reaction, it is concluded that there is no large influence of other reactions besides photoionizations. From the same reason, the effects of photo-electron cross currents among electrodes and recombination would be ignored. The electric field distortion near the photon entrance hole were not observed in this experiment so far as over 2 keV photons are introduced. In the case low energy photons are included, they interacts with gas near the entrance hole and might be accumulated in the vicinity and distort the electric field. This is beyond this calibration experiment.

In summary, it is concluded that the ICDE works well for measuring a broad spectrum of X-ray in the energy from 2 to 5 keV.

References

1) "Photon Cross Section from 0.1 keV to 1 MeV for Elements Z=1 to Z=94" Atomic Data 5, 51-111(1973)
2) M. Fukao, X-Ray Production in 1 keV Range and its Measurement: Journal of Plasma and Fusion Research, Vol. 73, No. 9(1997), pp. 912 - 922(in Japanese)
3) T. Murata et al., Soft x-ray beamline BL7A at the UVSOR: Rev. Sci. Instrum. 63(1), January 1992
4) T. Kinoshita et al., Focusing mirror system of the double crystal monochromator beamline Bl7A: UVSOR Activity report(1997)p. 62

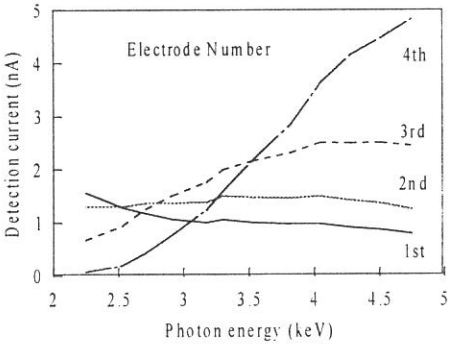

(a) observed

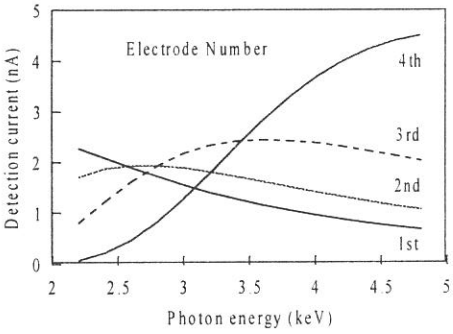

(b) theoretically expected

Fig.4 Photon energy vs. currents into the 4 electrodes (beam current : 100 mA)

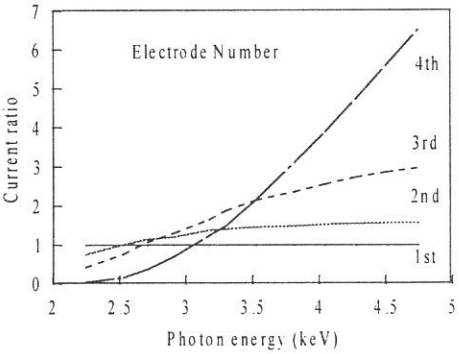

(a) observed

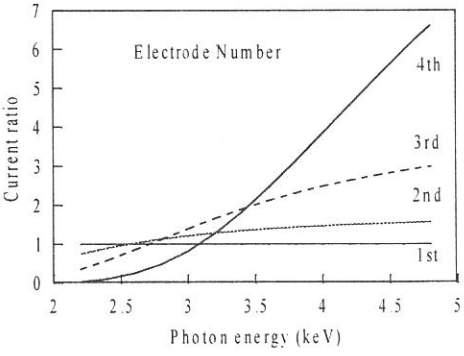

(b) theoretically expected

Fig.5 Photon energy vs. current ratios

BL-7A

Characterization of the Au and Pt replica mirrors for ASTRO-E

Kazutoshi Haga, Koujun Yamashita, Keisuke Tamura, Yasushi Ogasaka, Hideyo Kunieda, Yuzuru Tawara, Akihiro Furuzawa, Takashi Okajima, Harumi Takata, Seiji Takahashi, Satoshi Ichimaru, Yasuhiro Hidaka

Department of Physices, Nagoya University, Chikusa-ku, Nagoya 464-8602

X-ray astronomy satellite ASTRO-E will be launched in 2000. This satellite is equipment with five grazing incidence X-ray telescopes(XRT) coated with Au or Pt. X-ray imaging spectrometer(XIS) and X-ray spectrometer are installed on the focal plane, in order to observe the celestial objicts in the energy range 0.5 – 12keV.

XRT is made of 175 nested thin foil reflectors [1] per one telescope. The reflector is called "replica foil mirror " whose substrate is 0.15mm thick Al foil. The mirror is produced with replication of the gold or platinum sputtered on the glass mandrel with smooth surface.

The gold surface is a traditional material for total reflection and is prepared for XIS. On the other hand, Pt is used to extend the critical energy for the first time, because the density of Pt is higher than Au, the critical energy become larger in proportion to the square root of the density approximately.

Henke et al. reported the optical constants of various bulk materials including Au and Pt in 1982, 1993 [2,3]. But Owens et al.[4] reported that the M_V, M_{IV}, M_{III} edges of Au determined in reflecctivity measurements are about 30eV higher than Henke's value.

It is very important to know the optical constants of Au and Pt replica mirrors especially around the M edges in calculating XRT energy responces. Therefore the charactetization was carried out using monochromatized synchrotron radiation in the energy band 1.8 – 3.5keV including the M edges of Au and Pt.

Experiments were carried out in BL-7A. Incident beam was monochromatized by a double crystal monochrometer with InSn, and then introduced into the measuring chamber through the 0.2mmϕ pin-hole and filters to adjust the intensity and to calibrate the energies by using an absorption edge. The samples and the detectors(Proportional counter or Si detector) were mounted on the $\theta - 2\theta$ table in the chamber. First we measured the direct wavelength profiles in the energy range 1.8 3.7 keV. Next we obtained the reflected ones with the several incident angles.

Reflecivity of Au and Pt are shown in Fig.1, Fig.2. Energy calibration was carried out using K edge(3.2059keV) of Ar in the proportional counter, L edge(2.5202keV) of Mo in the filter, K edge(1.8389keV) of Si in the float glass reflector. These energies are refered from Henke's table.

Solid lines indicates the calculated value with rms roughness $\sigma = 5\mathring{A}$ which is defined as Debye-Wallar factor. It seems that absolute values of reflectivity are a little different from measured data. This is due to fluctuation of beam intensity within 0.2mmϕ pin-hole caused by the unstability of beam profile. For more accurate measurements in the future, we are considering a thin proportional counter of transparent type on the beam just in front of the sample, in order to monitor the incident flux.

From these measurements, M edge energies are determined as shown in Table.1 . Data summerized by Henke are also shown in Table.1 as a reference. These edge energies of Au in our measurements are similar to Owens's. As for Pt, the edge energy also has a tendency to be higher than Henke's as OWENS has listed. We would say that these results are very important and they shold be confirmed by other method such as transmission measurements.

material	M_V(eV)	M_{IV}(eV)	M_{III}(eV)
Au	2246±5(2205.7[3], 2241[4])	2331±5(2291.1[3],2329[4])	2747±5(2743.0[3],2756[4])
Pt	2160±5(2121.6[3],2154[4])	2235±5(2201.9[3],2234[4])	2641±5(2645.4[3])

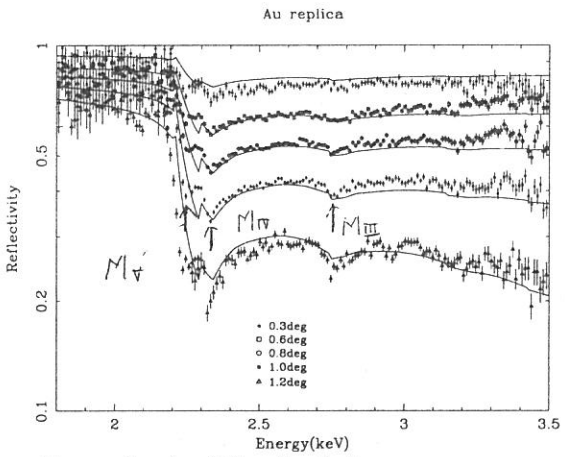

Figure 1: Au foil reflectivity: Solid line shows the calculated value. Measured data at the grazing angle of 0.3, 0.6, 0.8, 1.0, 1.2degree are shown.

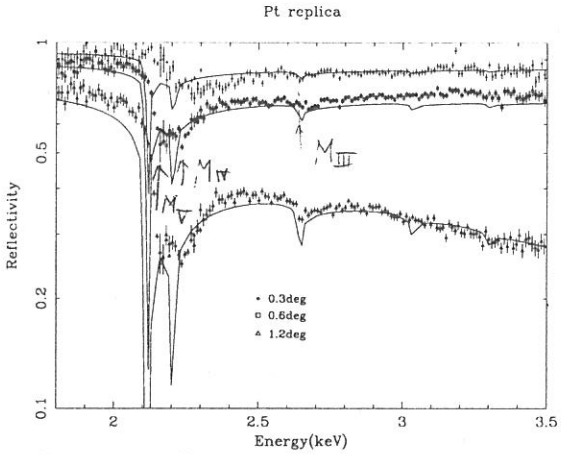

Figure 2: Pt foil reflectivity: Solid line shows the calculated value. Measured data at the grazing angle of 0.3, 0.6, 1.2degree are shown.

references

1) Peter J. SERLEMITSOS, et al. 1995, Publ. Astron. Soc. Japan 47, 105-114
2) HEKNE, B.L., et al. 1982, Atomic Data Nucl. Data Tables, 27, 1
3) HEKNE, B.L., et al. 1993, Atomic Data Nucl. Data Tables, 54, 1
4) OWENS, A., et al. 1996, ApJ, 468, 451

(BL-7A)

Structure of Impurity Si Atoms in α-Al_2O_3 Crystal by XAFS Spectroscopy.

Kohei Fukumi, Naoyuki Kitamura, Hiroshi Mizoguchi

Osaka National Research Institute, AIST
1-8-31, Midorigaoka, Ikeda Osaka, 563-8577 Japan

Optical properties of inorganic materials are much affected by impurities. In order to underdstand the optical properties of these materials, it is important to know the coordination structure and valence state of impurity atoms in the materials. In this study, the structure of Si atoms in α-Al_2O_3 has been investigated by XAFS spectroscopy.

α-Al_2O_3 single crystal including Si atoms as an impurity atom was used as a sample. β-SiC powder, α-Si_3N_4 powder, α-quartz type SiO_2 powder and Si single crystal were used as reference substances. The measurement of Si K-edge XAFS spectra of these samples was carried out on the beam line 7A at UVSOR facility, Institute for Molecular Science, Okazaki, Japan. The spectra of the Si-doped Al_2O_3 single crystal, silicon compound powders and Si single crystal were measured by electron yield, total electron yield and drain current methods, respectively. In addition, the Si K-edge XAFS measurement was carried out on the Si-doped Al_2O_3 single crystal with a photodiode(AXUV-100,IRD Inc.). All the spectra were measured at room temperature using an InSb double crystal monochromator.

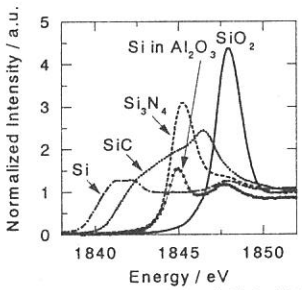

Fig.1 XANES spectra of Si in Al_2O_3, SiO_2, Si_3N_4, SiC and Si.

Figure 1 shows the Si K-edge XANES spectra of Si atoms in Al_2O_3 single crystal, SiO_2, Si_3N_4, SiC and Si. The edge energy shifted toward higher energies in the order of Si<SiC<Si_3N_4<SiO_2. This agrees well with the order of ionic charge of Si atoms. The edge of Si atoms in α-Al_2O_3 located at the energy of Si_3N_4, indicating that the ionic charge of Si atoms in α-Al_2O_3 is less than that of Si atoms in SiO_2.

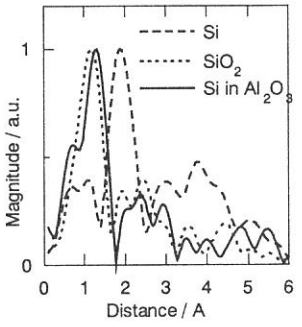

Fig.2 Magnitude of fourier-transform of kχ(k) of Si in Al_2O_3, SiO_2 and Si. Magnitude is normalized to unitiy.

Figure 2 shows the magnitude of fourier-transform of kχ(k) obtained from XAFS measurement. It can be seen that the most intense peak of Si atoms in α-Al_2O_3 locates at a position similar to that in SiO_2, indicating that Si atoms are mainly surrounded by oxygen atoms. The Si-O bond length in α-Al_2O_3 and SiO_2 was 1.67Å and 1.60Å, respectively, according to the fitting analysis in the region from 3.2 to 8.0$Å^{-1}$, although the k range of kχ(k) curves used for the fitting analysis was too narrow to discuss the bond length precisely. Oxygen atoms have the hexagonal closest packed structure to form tetrahedral sites and octahedral sites in α-Al_2O_3 crystal. It is deduced from the Si-O bond length that Si atoms occupy the tetrahedral site in α-Al_2O_3 crystal.

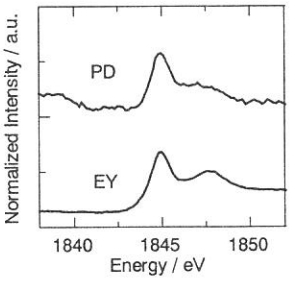

Fig.3 XANES spectra of Si atoms in Al_2O_3 measured by electron yield (EY) and photodiode (PD) methods.

Figure 3 shows that XANES spectra of Si atoms in α-Al_2O_3 measured by the electron yield method and the photodiode method. It was confirmed that XANES spectrum of dilute components can be measured by the photodiode method.